8-9-2019

Analysis of individual molecular dynamics snapshots simulating wetting of surfaces using spheroidal geometric constructions

Aleksandr Abramov
Edith Cowan University

Stefan Iglauer
Edith Cowan University

10.1063/1.5113852

Analysis of individual molecular dynamics snapshots simulating wetting of surfaces using spheroidal geometric constructions

Aleksandr Abramov*, Stefan Iglauer, School of Engineering, Edith Cowan University, 270 Joondalup Drive, Joondalup, WA 6027, Western Australia, Australia

*aabramov@our.ecu.edu.au

Abstract

Accurate characterisation of wettability of minerals is important for efficient oil recovery and carbon geo-sequestration. In studies where molecular dynamics simulations are used to compute the contact angle, emphasis is often placed on results or theoretical details of the simulations themselves, overlooking potentially applicable methodologies for determination of the contact angle. In this manuscript a concept of a method utilizing spheroidal geometric constructions to estimate the contact angle of a water droplet on silica surface in carbon dioxide atmosphere is outlined and applied to the final snapshots of two molecular dynamics simulation runs. Two carbon dioxide pressures and two wettability modes (hydrophilic and hydrophobic) are examined to assess the method's performance. The most stable 6-member ellipse-like rings (001) pristine surface of alpha-quartz is reconstructed using molecular dynamics and its wettability is then investigated for the first time. The outcomes of the calculations are compared with results produced with the iso-density chart method; and good agreement with the latter approach is demonstrated. The proposed method can be used as an alternative, or in conjunction with other techniques, to increase the confidence in contact angle estimations via molecular mechanics calculations. Reliable contact angle estimations on the other hand, can guarantee accurate storage capacity and security of carbon capture and storage projects.

Key words: contact angle, molecular dynamics, simulation snapshot, wettability, spherical droplet

Introduction and motivation

Carbon capture and storage is a recognized technology that reduces concentration of carbon dioxide in the Earth's atmosphere [1]. Storage capacity and security of formations used to store CO_2 depend on wettability of minerals [2-3], specifically quartz in carbon dioxide environment, which was studied experimentally and theoretically [4].

There are number of works employing molecular dynamics to simulate the wetting behaviour of water on silica surfaces, in particular in the presence of carbon dioxide and often in the context of carbon geo-sequestration [5-17]. In some studies, formation of the meniscus between two slabs is modelled [6], in others a cylindrical droplet is used [14]. While these approaches offer smaller system sizes and less demanding computations, they may miss important wetting features, like preferential wetting directions on some surfaces [18]. With increasing computational power of modern computers these techniques become less popular, thus the majority of researchers directly simulate a water droplet on the solid surface and further analyse the results [5, 7-9, 12].

However, the analysis of such simulation results is often limited to two-dimensional structures. From these, the contact angle is determined via second order polynomial fits to the two-dimensional water droplet profile [5], or via drawing contours around two-dimensional water density plots [6-9, 12].

These approaches are local, thus only a certain part of the droplet's profile cross section is considered. When tangential lines are fitted, the three-dimensional nature of the studied systems is lost, which introduces a bias (when projecting three-dimensional objects into two-dimensional space). The approaches lack appreciation of the physico-chemical aspects of droplet formation in the simulation environment. By the latter we mean that in absence of gravity the system (water droplet) which is destined to minimize its surface energy (and thus the surface area) unavoidably adopts spheroidal shape. In some developments, three-dimensionality of spheroidal droplets was taken into account, with water density profiles constructed in cylindrical coordinates, with further fitting of two-dimensional circles to these profiles [7]. In a rigorous analysis based on the coarse-grained density of

fluid molecules [19], the average liquid-vapour interface is set at the half of the bulk liquid density. The contact angle is then calculated using two methods the spherical-cap approximation and the outward unit normal to the interface. In the spirit of this latter study we use the most natural geometrical constructions and a coordinate system for spherically shaped objects, i.e. spheroidal constructions and the spherical coordinate system. Unlike the method outlined in [19], which makes use of position vector dependent coarse-grained fluid density, our approach uses spherical shell averaged fluid density which is a function of the radius vector. This deviation requires different methodological and algorithmic tactics for the method to be simple and work successfully. In this work we thus have a twofold goal. Firstly, we argue that a holistic method to estimate the contact angle can be developed that (i) treats the overall droplet in three dimensions, based on the spherical coordinate system, and (ii) respects intrinsic physics and the resulting geometry of the simulated structures using spheroidal geometric construction. Secondly, we enrich and continue debate on the performance of the approaches used to compute the contact angles and on the rational choice of parameters used in these approaches.

To this end we use a water droplet on a pristine (001) α-quartz surface in carbon dioxide environment under 4 and 10 MPa pressure and at 300 K temperature. The pristine quartz surface was previously modelled and reconstructed in [20-24]. According to available information in the literature the pristine surface has two energetically very similar structures the 6-member triangle-like rings and the 6-member ellipse-like rings. To the best of our knowledge the latter and the most stable structure was predicted in [20]. It was then studied in [22-24], with experimental confirmation reported in [22]. As far as the authors of this paper are concerned, there are no reports where the most stable 6-member ellipse-like rings pristine (001) α-quartz surface is explicitly mentioned in the context of its wettability or reconstructed using classical molecular dynamics.

Method development

Development of the method that is based on the spherical coordinate system requires identification of the smallest radius of a sphere which encapsulates all water molecules of the droplet. If position of this sphere's centre is known, its radius can be easily calculated as the distance to the furthest water molecule. It is thus necessary to find the location of the smallest circumscribing sphere. As it will be clear from the following discussion this is valid for hydrophobic surfaces; with some minor alterations the approach can then be generalized to also include hydrophilic surfaces.

The radius of the circumscribing sphere depends on the position of its centre, and it is reasonable to assume that the centre of the minimal radius sphere lies on a normal of the surface which intersects the centre of mass of the droplet. To find the exact position of the centre we introduce the following scanning algorithm, see Figure 1. Suppose that the vertical line through the centre of mass of the water droplet is found as a locus of points with x and y coordinates of the mass centre. We select a step which divides the line into integer number of segments, e.g. hundredth of the cell height. We loop over every point between segments. For every point we find a distance to every atom of all molecules comprising the water droplet. The largest distance is taken as the encapsulating radius corresponding to the given point. The smallest radius identified is the radius of the sphere we are looking for, and the position of the sphere's centre is the position of the point to which this radius corresponds. We next narrow down the search interval by taking one step backward and one step forward from the point found. We divide this interval by the same number of steps and repeat the search. We keep narrowing down the interval until the step size is below a given accuracy threshold, in this work the threshold 10^{-6} A is used.

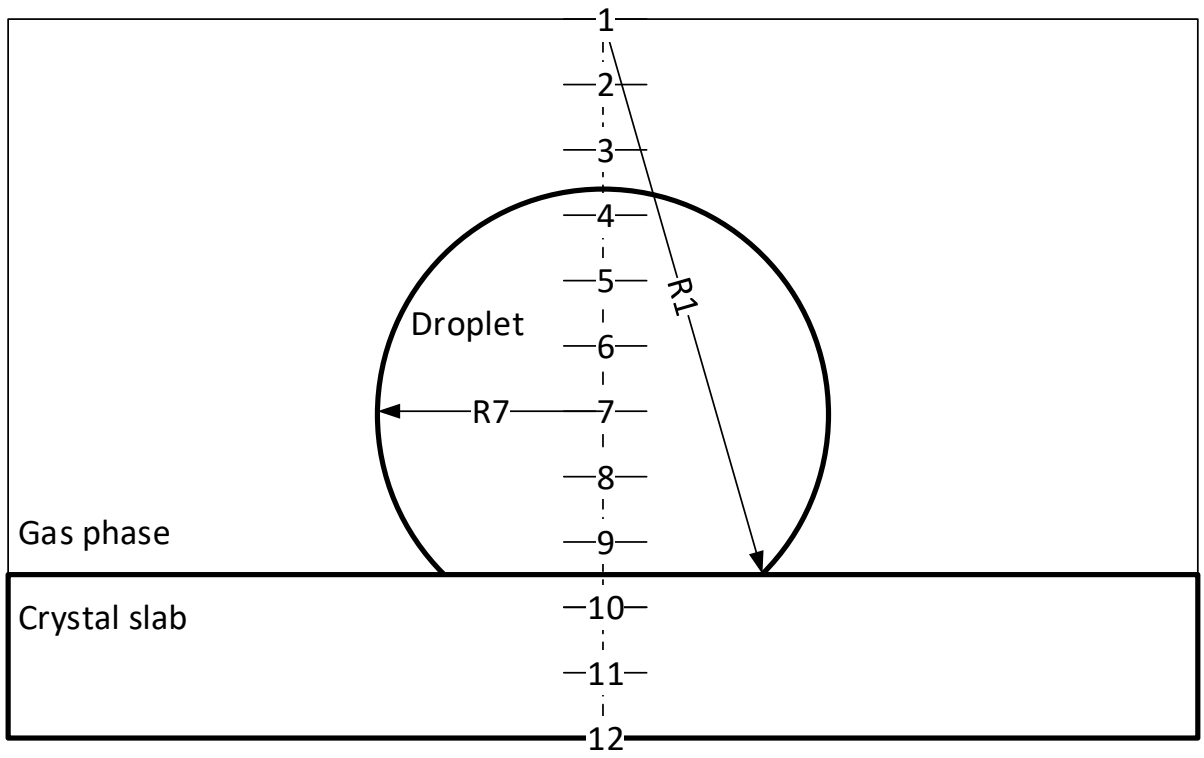

Figure 1. Simulation cell with schematic illustration of hydrophobic surface, water droplet and steps of the scanning algorithm.

The described procedure is exemplified for 12 initial steps in Figure 1. The radii of spheres encapsulating the droplet for steps 1 and 7 are shown as R1 and R7. In the first pass R7 is going to be identified as the smallest droplet encapsulating radius. In the second pass the search interval is going to be narrowed down to the interval between points 6 and 8. In this particular example the radius shown as R7 is going to remain the smallest encapsulating radius until the algorithm reaches the threshold value for the search interval. In a more general case the smallest encapsulating radius is refined over the course of algorithm execution. It is worth noting that there is no need to scan the whole cell. Obviously, the centre of the sphere is inside the droplet, so one only needs to scan from the top of the droplet to its bottom.

For hydrophilic surfaces the above described algorithm finds the wetted radius of the droplet (R_w), see Figure 2. With known droplet height (H_d) this value can be used to identify the position of the centre of the circumscribed sphere (Z_r) and its radius (R):

$$Z_r = Z_{top} - R,$$

$$R = \frac{R_w^2 + H_d^2}{2H_d}.$$

To obtain the latter expression note that in the hydrophilic case, see Figure 2:

$$R^2 = R_w^2 + (R - H_d)^2.$$

For the sake of completeness, it is worth noting that for any two points on circle's contour (R_1, Z_1) and (R_2, Z_2) within one quadrant, not just (0, Z_{top}) and (R_w, 0), a more general expression for the position Z_r can be derived:

$$Z_r = \frac{R_2^2 + Z_2^2 - R_1^2 - Z_1^2}{2(Z_2 - Z_1)}.$$

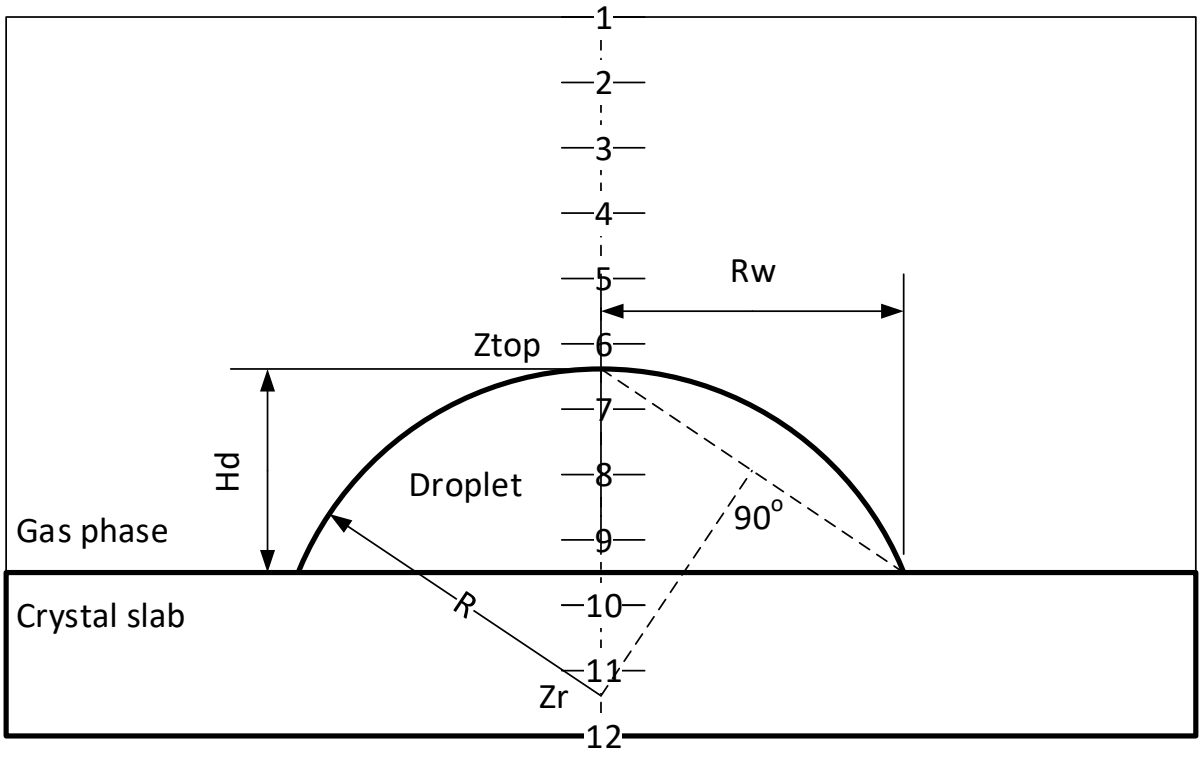

Figure 2. Simulation cell with schematic illustration of a hydrophilic surface, showing the water droplet, steps and elements of the scanning algorithm.

However, in actual simulations droplets rarely resemble perfect spheres or spherical caps. It is thus necessary to refine the radii found. This refinement is done for both, the wetted radius (hydrophilic

case) and the radius of the circumscribed sphere. For the latter one we construct density plots in spherical coordinates by changing the radius from zero to R in small steps dR and calculating the number of molecules in the spherical shell between R and dR, see Figure 3. For a hydrophobic surface the volume of the spherical shell is equal to the volume of a sphere of radius R+dR minus the volume of the sphere of radius R, and minus volume of the spherical cap. For a hydrophilic surface the volume of the spherical shell is equal to the volume of the spherical cap. The spherical cap, just as the spherical shell, is spatially limited between radii R and R+dR. The threshold density, i.e. the density where the water droplet ends (or starts), is assumed to be half the normal water density. The exact figure is taken as 0.033/2 water molecules per cubic angstrom, which corresponds to half of normal water density 1000 kg/m^3. Example plots of the water density in spherical coordinates are illustrated in Figure 8 and Figure 9. To refine the wetted radius in the hydrophilic case we use an analogous procedure with the only difference being that the cylindrical coordinates are used instead of spherical coordinates. The location of the thin cylinder is at the z coordinate of the radius and its thickness is taken to be 3 A, close to the mean van der Waals diameter of water[25]. The dR value is taken to be 0.25 A for both coordinate systems, the spherical and the cylindrical.

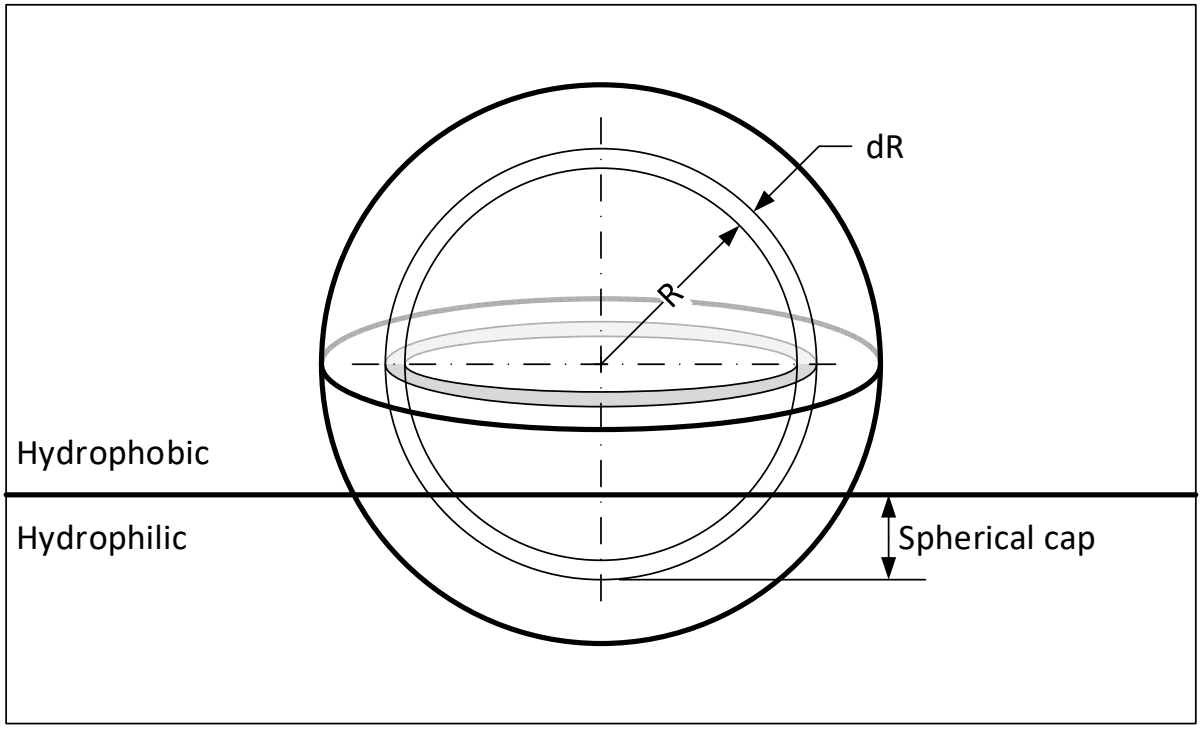

Figure 3. Calculation of water density in spherical coordinates for hydrophobic and hydrophilic surfaces.

When the radius of the water molecules encapsulating sphere, and its position relative to the surface are known calculations of the contact angle become trivial, see Figure 4. With Z_{top} measured from the surface, for the hydrophobic case the contact angle θ is given by:

$$\theta = 180° - \alpha,$$

$$\cos\alpha = \frac{Z_{top} - R}{R}.$$

And for the hydrophilic case the contact angle is:

$$\theta = \alpha,$$

$$\sin\alpha = \frac{R_w}{R}.$$

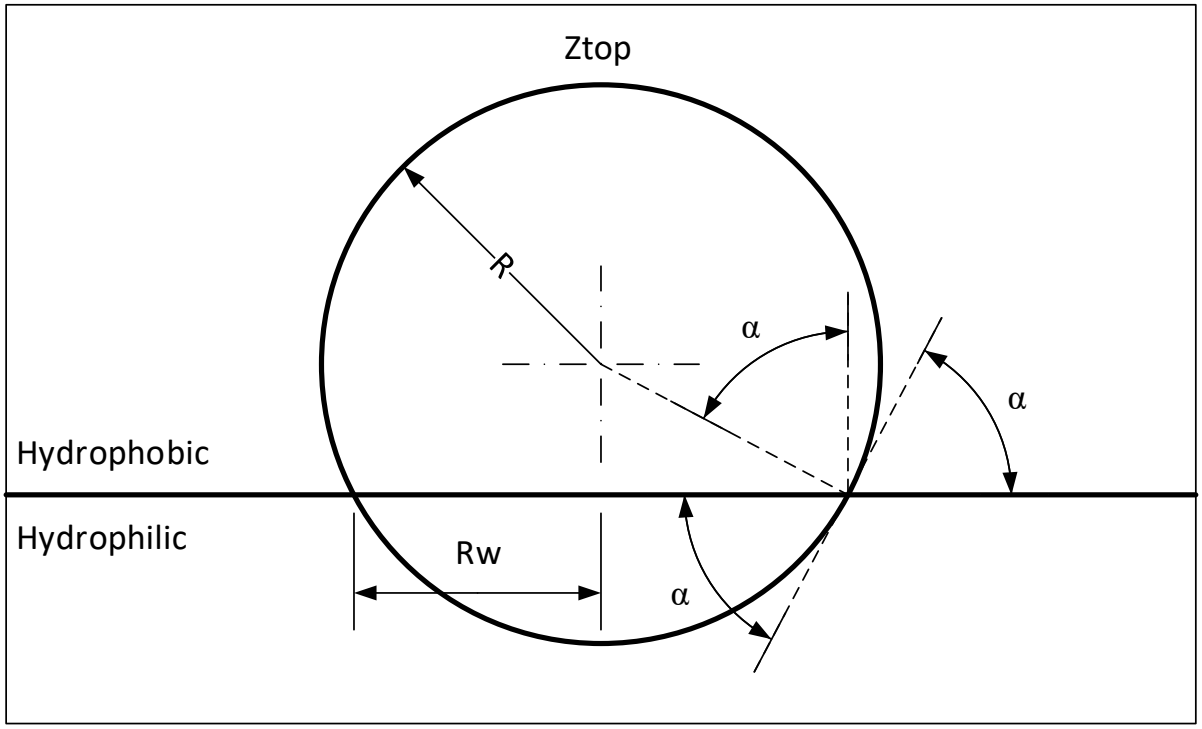

Figure 4. Illustration of contact angle calculations.

As treatment of hydrophilic and hydrophobic surfaces is different, it is important to distinguish between them. Thus the following inequality is used to decide if the surface is hydrophilic,

$$R > H_d.$$

Note that the formulae written in terms of Z_{top} can easily be rewritten in terms of the position of the centre of the circumscribed sphere once it has been found.

Contact angles computed with the circumscribed sphere method are compared with results obtained from the iso-density chart method. In the latter method the droplet is divided into thin circular layers, the thickness is taken to be 0.25 A; in each layer the water density is calculated in the cylindrical coordinate system starting from well outside of the droplet, i.e. the density is calculated in thin rings with dR=0.25 A. By proceeding towards the droplet centre the position of iso-density 0.033/2 water molecules per cubic angstrom is identified in each layer. The resulting line connecting all obtained data points plotted in coordinates height versus radius contours the extent of the droplet, see Figure 12 and Figure 13 for the example. The average radius of the lowest two points is used to set the

intersection of the tangential line with the horizontal axis. The next 5, 7 and 9 data points are used to fit the tangential lines to the iso-density and thus three contact angles are determined. An average (over the three values) contact angle is compared with that obtained with the circumscribed sphere method. Note that in both methods, when calculating water density profiles, the positions of the water molecules are approximated by positions of the oxygen atoms.

Computational details

A general purpose parallel molecular dynamics simulation package DL_POLY 4.08 was applied to perform computations [26-27]. Results of the simulations were visualized with VMD [28] and VESTA [29] software, the latter one was also used for manipulations with molecular and periodic structures.

In all classical molecular dynamics simulations integration of the equations of motion was performed with the velocity Verlet algorithm [30]. The time step in all simulations was set to 2 fs. In the NPT simulations the Nose-Hoover thermostat and barostat [31-32] with the relaxation constants 0.05 and 0.5 ps, respectively, were used. In the NVT simulations the Nose-Hoover thermostat with the relaxation constant 0.05 ps was used. Interactions cutoff distance was set to 17 A in all calculations. Electrostatics were computed with the smoothed particle mesh Ewald summation [33-34].

Force fields

A set of force fields was employed in this study. The BKS (van Beest, Kramer, Santen) potential [35] was used for the pristine quartz surface. The potential was coupled with the TIP4P/2005 model for water [36] and the EPM2 model for carbon dioxide [37]. Only non-bond potential terms were utilized, with all H_2O and CO_2 molecules being treated as rigid bodies. Geometrical details of the rigid bodies are: CO distance (EPM2 CO_2) 1.149 A; OH distance (TIP4P/2005 H_2O) 0.9572 A; OM distance (TIP4P/2005 H_2O) 0.1546 A; HOH angle (TIP4P/2005 H_2O) 104.52°.

The Buckingham potential [38] was used to model oxygen-oxygen and silicon-oxygen interactions of the pristine quartz surface:

$$U(r) = Aexp\left(-\frac{r}{\rho}\right) - \frac{C}{r^6},$$

where U is the potential energy of interacting atoms separated by the distance r; A, ρ and C are the parameters of the potential, see Table 1. All silicon-silicon interactions were modelled with electrostatic forces only.

Table 1. The Buckingham potential parameters used for the pristine quartz surface [35].

Interactions	A, kcal/mol	ρ, A	C, kcal/mol A^6	q, e	m, amu
O-O	$3.20304 \cdot 10^4$	0.3623188	$4.03609 \cdot 10^3$	O=-1.2	O=15.9994
Si-O	$4.15225 \cdot 10^5$	0.2052124	$3.07983 \cdot 10^3$	Si=2.4	Si=28.0855

The Lennard-Jones potential was used to model dispersion interactions of water, carbon dioxide and the ions for the pristine quartz surface:

$$U(r) = 4\varepsilon\left[\left(\frac{\sigma}{r}\right)^{12} - \left(\frac{\sigma}{r}\right)^{6}\right].$$

Parameters of the potential ε and σ are given in Table 2.

Table 2. The Lennard-Jones potential parameters used to model CO_2-H_2O-SiO_2 systems [7, 35-37].

Atomic sites	ε, kcal/mol	σ, A	q, e	m, amu
C (CO_2)	0.05591	2.757	0.6512	12.0107
O (CO_2)	0.16001	3.033	-0.3256	15.9994
O (H_2O)	0.18523	3.1589	0	15.9994
H (H_2O)	0	0	0.5564	1.0080
M (H_2O)	0	0	-1.1128	0
Si (SiO_2)	0.12751	3.795	2.4	28.0855
O (SiO_2)	0.15504	3.154	-1.2	15.9994

The interaction parameters between the unlike atoms were obtained as the geometric mean for the energy parameter and as the arithmetic mean for the distance parameter (the Lorentz-Berthelot combining rules [39-40]):

$$\varepsilon_{ij} = \sqrt{\varepsilon_i \varepsilon_j},$$

$$\sigma_{ij} = (\sigma_i + \sigma_j)/2,$$

where i and j are indices of the unlike atoms.

Reconstruction of the pristine quartz surface

From the hexagonal unit cell of α-quartz [41] shown in Figure 5 a super cell 2x2x1 was created. An orthorhombic cell for further preparation of the pristine surface was then extracted from the super cell [42], see Figure 5. There are 18 atoms in the orthorhombic cell, 6 silicon atoms and 12 oxygen atoms.

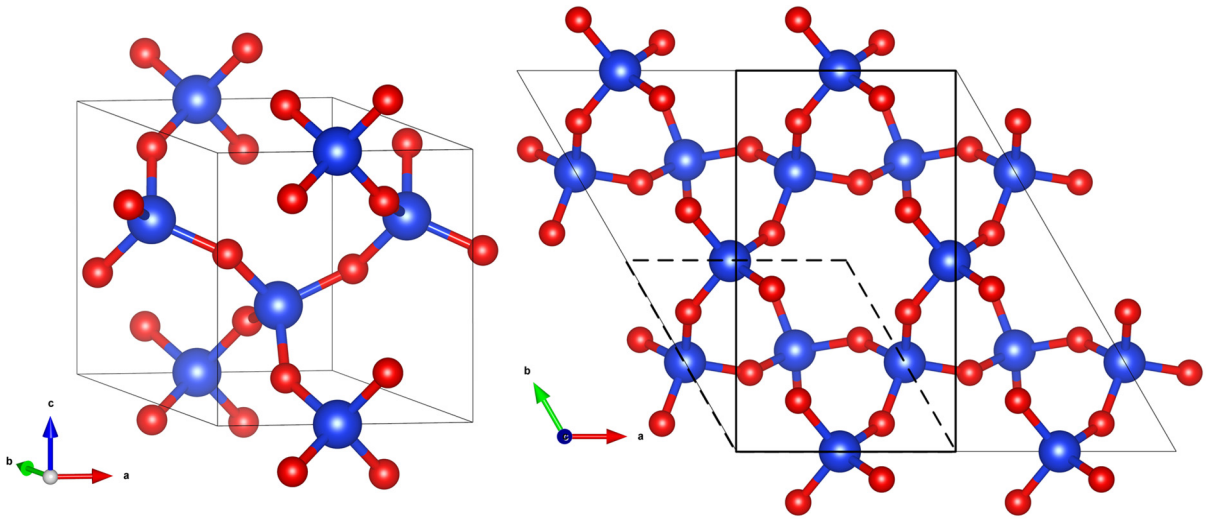

Figure 5. Quartz unit cells used in this work. Left: primitive hexagonal unit cell of α-quartz, isometric view. Right: reconstruction of the orthorhombic cell (solid bold rectangle) from 2x2x1 super cell, top view (dashed parallelogram shows the primitive cell). Red balls - oxygen atoms, blue balls - silicon atoms.

Crystallographic lattice vectors of the orthorhombic cell amount to: a=4.916 A, b=8.515 A, c=5.405 A. Out of this orthorhombic cell a super cell 12x7x12 was constructed and used to equilibrate the quartz crystal at 1 atm pressure and 300 K temperature for 10^5 steps. The system was simulated in the NPT ensemble. Lattice vectors of the equilibrated orthorhombic cell were found to be a=4.940 A, b=8.557 A, c=5.432 A, which are only 0.5% larger than the crystallographic values obtained from [41]. Using this equilibrated orthorhombic cell a 20x12x4 slab was constructed. Every uncoordinated oxygen atom at the top of the slab was shifted from the host silicon atom towards the neighbouring silicon atom in x and y directions by 0.6 A to build precursors of the Si-O-Si bridges. After that the slab

was relaxed at 10 K for 10^5 steps to form proper Si-O-Si bridges and the initial ordered surface structure. The system was simulated in the NVT ensemble. During the relaxation and in all subsequent simulations described in this work the bottom layer (in terms of the unit cell height) of the four-layer slab was kept frozen to emulate the bulk crystal. The surface was prepared in a simulation box which had the same dimensions as the box used for the fully assembled quartz-water-CO_2 systems. Arrangement of the very top atoms of the surface is the same as in the lowest energy surface obtained in [23-24]. The surface consists of 6-member ellipse-like rings, Figure 6.

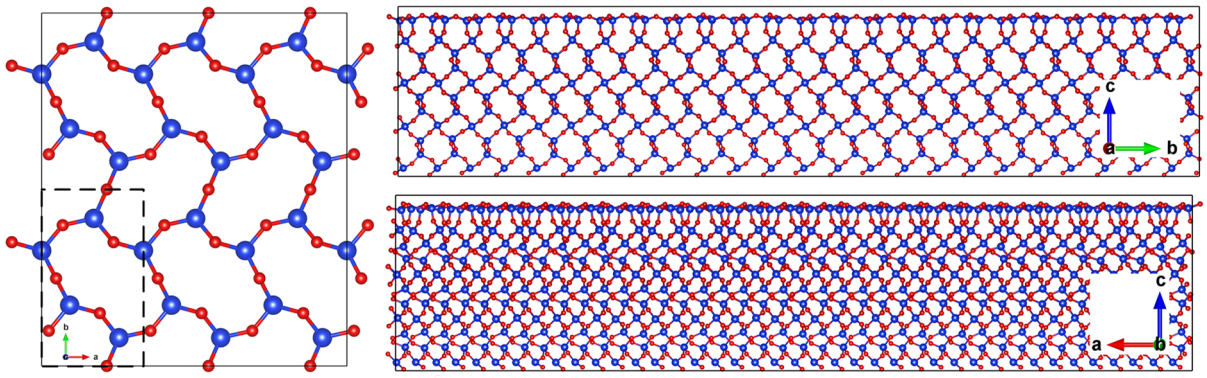

Figure 6. Four-layer quartz slab used in this work. Left: view of the super cell 3x2x1 along z direction with only top atoms shown for clarity (the orthorhombic unit cell is highlighted with dashed rectangle). Right: slab views along x (right top) and y (right bottom) directions. Red balls - oxygen atoms, blue balls - silicon atoms.

Simulation setups

Utilizing above described force fields and the pristine quartz surface two simulation models were constructed with two different carbon dioxide pressures (4 and 10 MPa). Temperature in all simulations was set to 300K. Preliminary equilibration of carbon dioxide and water with the subsequent construction of the models was performed.

Two boxes 120x120x80 A for carbon dioxide and 50x50x50 A for water (the TIP4P/2005 [36] were used to pre-equilibrate uniformly distributed molecules at 300K. Density of carbon dioxide at given pressure and temperature were used to determine the volume per every molecule, this density was taken from the NIST data book at 300 K and at the relevant pressures of 4 and 10 MPa [43]. Water density was taken to be 1000 kg/m^3. Dynamics of these three systems (one for H_2O and two for CO_2) were modelled in the NVT ensembles. Overall $5 \cdot 10^5$ steps were performed for CO_2 and 10^5 for H_2O.

On top of the pre-equilibrated quartz slabs a half sphere of radius 24 A was filled with water molecules from above described box. Overall 772 TIP4P/2005 water molecules fit into the half sphere. These "water droplets" were placed in the centre of the slabs. The rest of the space up to 60 A above the surface was filled with pre-equilibrated carbon dioxide. There were 642 and 5559 CO_2 molecules above the pristine surface at 4 and 10 MPa, respectively. A gap of 1.5 A starting from four quartz unit cell heights (the slab's height) was left empty to avoid overlap of atoms and molecules. Note that actual initial distance between top slab atoms and water and gas molecules was slightly larger due to surface construction during relaxation and disposition of molecules in the pre-equilibration boxes, thus molecules located exactly at the border were rejected upon filling the simulation boxes. Vacuum space of 70 A was provided above the gas phase. All simulations were performed with periodic boundary conditions in x and y directions. In z direction a repulsive force was initially set at 60 A above from the surface:

$$F = k(z_0 - z), z > z_0,$$

where k=0.24 kcal/mol (1 kJ/mol) - is the force constant, and z_0 is the position of the repulsive potential.

The position of this repulsive wall was then corrected in such a way that the density of the pre-equilibrated carbon dioxide filling space above the surface matched its physical density at given pressure and temperature. In all cases the potential was never displaced towards the surface by more than 6 A, see Table 3. Minimal distance to the repulsive potential of more than 54 A ensures that the contact angle at the surface is not affected by perturbations in the CO_2 density caused by the wall.

Dynamics of two prepared quartz-water-carbon dioxide systems were simulated in the NVT ensembles. Overall 10^6 steps were performed for every system, 2 ns simulation time, out of which 10^5 were equilibration steps. Dimensions of the simulation boxes were 98.81x102.68x151.73 A. Figure 7 demonstrates the initial simulation setups for two studied systems. Main computational details are summarized in Table 3.

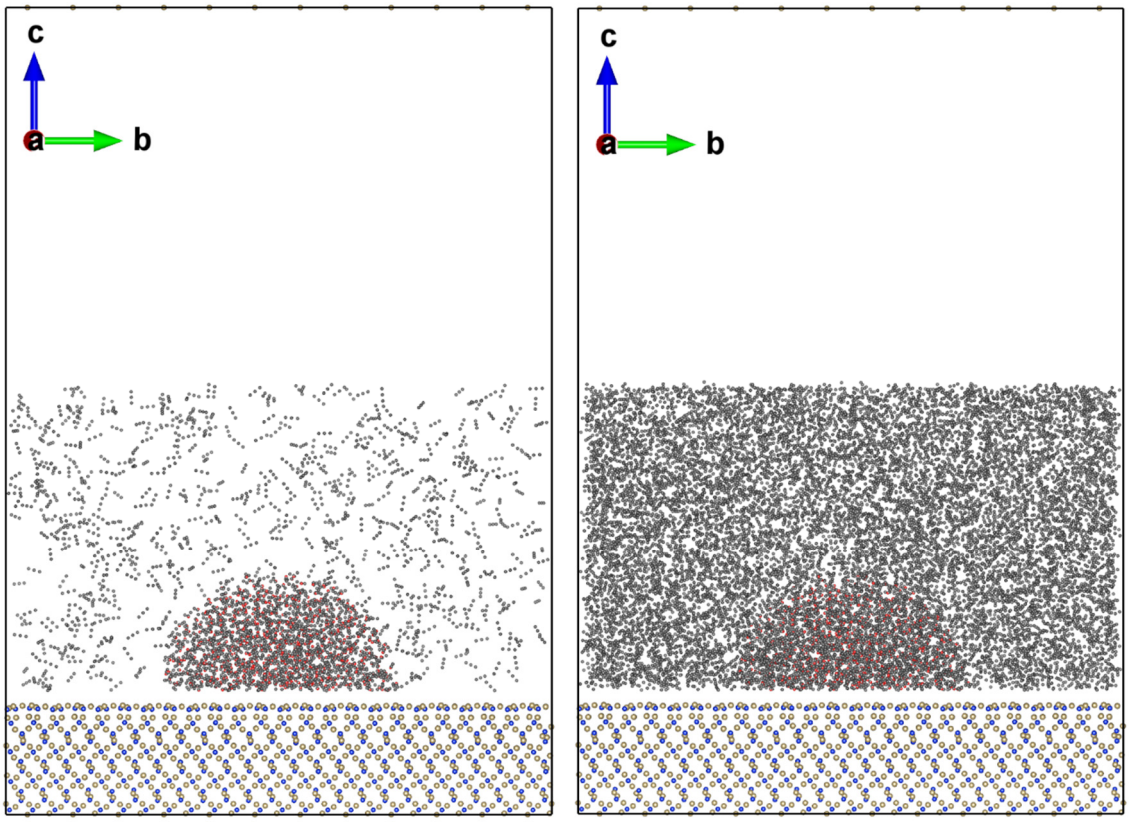

Figure 7. Initial simulation setups for systems investigated at two CO_2 pressures - 4 MPa (left) and 10 MPa (right). The hemispherical water droplets above the quartz surfaces surrounded by CO_2 molecules are clearly visible.

Table 3. Summary of computational details.

Parameters	System 1	System 2
CO_2 pressure, MPa	4	10
Temperature, K	300	
Force fields	BKS, TIP4P/2005, EPM2	
Interactions cutoff, A	17	
Time step, ps	0.002	
Number of steps (equilibration steps)	10^6 (10^5)	
Ensemble	NVT	
Thermostat	Nose-Hoover	
Thermostat relaxation constant, ps	0.05	

Parameters	System 1	System 2
Repulsive potential z_0, A	54.64	54.31
Repulsive potential k, kcal/mol	0.24	
Half sphere droplet radius, A	24	
H_2O molecules	772	
CO_2 molecules	642	5559
Slab top layer	240(Si_6O_{12})	
Slab two middle layers	480(Si_6O_{12})	
Slab frozen (bottom) layer	240(Si_6O_{12})	
Slab unit cell dimensions, A	4.94x8.56x5.43	
Slab dimensions in unit cells	20x12x4	
Simulation box dimensions, A	98.81x102.68x151.73	

Method application and discussion

For both systems investigated the very last snapshots of the simulations were analysed using above described methodology. Obtained results of the contact angle analysis are summarized in Table 4.

Table 4. Contact angle computational results.

Initial simulation setup	System 1	System 2
CO_2 pressure, MPa	4	10
Circumscribed sphere radius, A	31.375	22.125
Position of sphere's centre with respect to the surface, A	-12.82	1.88
Contact angle (circumscribed sphere method), degrees	65.9	94.9
Contact angle (iso-density chart method), degrees	69.0 (+/-4.7)	92.6 (+/-2.6)

It is noteworthy to see how the two methods, the circumscribed sphere method and the iso-density chart method, arrived at essentially the same results using different routes. The largest discrepancy in found contact angles is in the range of 5%. Thus, the surface at 4 MPa of CO_2 pressure is hydrophilic

(the contact angle is less than 90°), the surface at 10 MPa of CO_2 pressure is slightly hydrophobic (the contact angle is more than 90°). As required by the initial formulation of the problem of this study we are working here with individual molecular dynamics snapshots. Thus comparison between two used here methods is valid and significant. Comparison with previously reported simulation results [7], which used the same simulation length (2 ns) on the other hand can be indicative of relative wettability of the most stable 6-member ellipse-like rings (001) pristine surface of α-quartz. Our computed contact angles are in reasonable agreement with previously reported simulation data where the contact angles were found to be 69° and 80° at 300 K and 4 and 10 MPa of CO_2 pressure, respectively [7]. Higher contact angle at 10 MPa of CO_2 pressure calculated in this work shows that the most stable 6-member ellipse-like rings (001) pristine surface of α-quartz is more hydrophobic than the 6-member triangle-like rings surface used in [7]. Additional comparison with experimental results can validate used theoretical assumptions and approximations. In an experimental study conducted at 298 K, during repeated exposure to CO_2, the contact angles of water droplets on quartz substrates were found to be 90° and 80° at 4 and 10 MPa of pressure, respectively [44], which are similar to obtained here values.

It should be noted here that simulations executed in this work are organized such that the initial atomic configurations are close to the equilibrium (the contact angle of the hemispherical droplet is 90°, c.f. to computed above 65.9° and 94.9°). In addition to this, all elements of the initial setups (the slab, CO_2, water molecules of the droplet) are relaxed and pre-equilibrated. It thus follows that 2 ns simulation time is sufficient for statistically significant results extracted from a single simulation snapshot. Quantitative validation for the latter statement can be produced using tails of generated trajectories. From the last 50 000 steps (0.1 ns simulation time) five simulation snapshots separated by 10 000 steps were extracted and the contact angles were computed using the circumscribed sphere method. For the systems at 4 and 10 MPa CO_2 pressure the contact angles amounted to 62.6° (+/-3.3) and 96.5° (+/-1.7), respectively. Small error bars indicate that the systems are well equilibrated and obtained results used for comparison with works mentioned in the previous paragraph are significant.

Water density profiles constructed in spherical coordinates are shown in Figure 8 and Figure 9. Approaching the spheres' centres from the infinity, the threshold water density (0.033/2 water molecules per cubic angstrom) signals where the droplets start. A common feature of both plots is relatively slow increase in the density in the beginning and its abrupt decrease in the end. A slow threshold approach makes refinement of droplets' radii relatively reliable, as the density increases from zero to 0.033/2 water molecules per cubic angstrom over the distance of several angstroms.

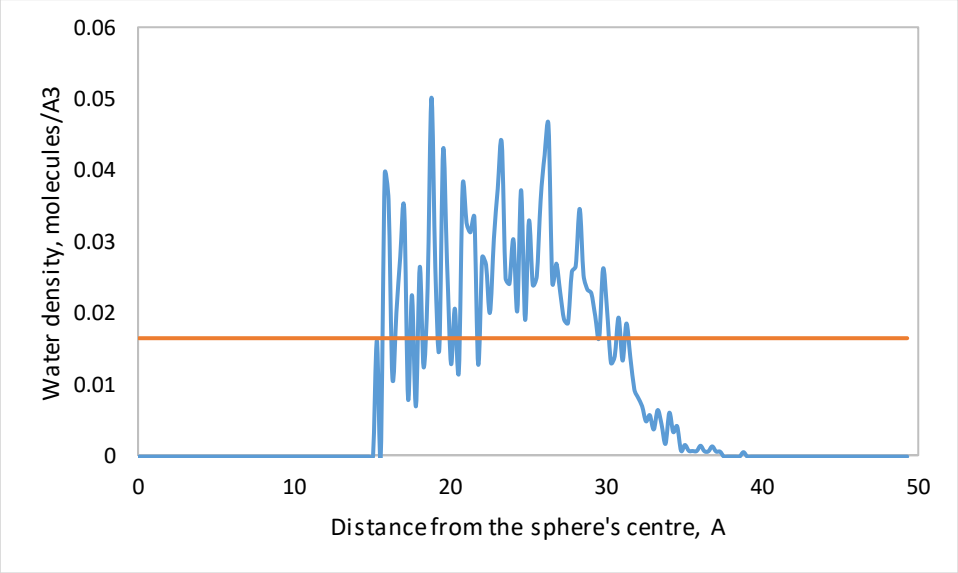

Figure 8. Water density in spherical coordinates for the system at 4 MPa CO_2 pressure. Horizontal line shows half of water's normal density.

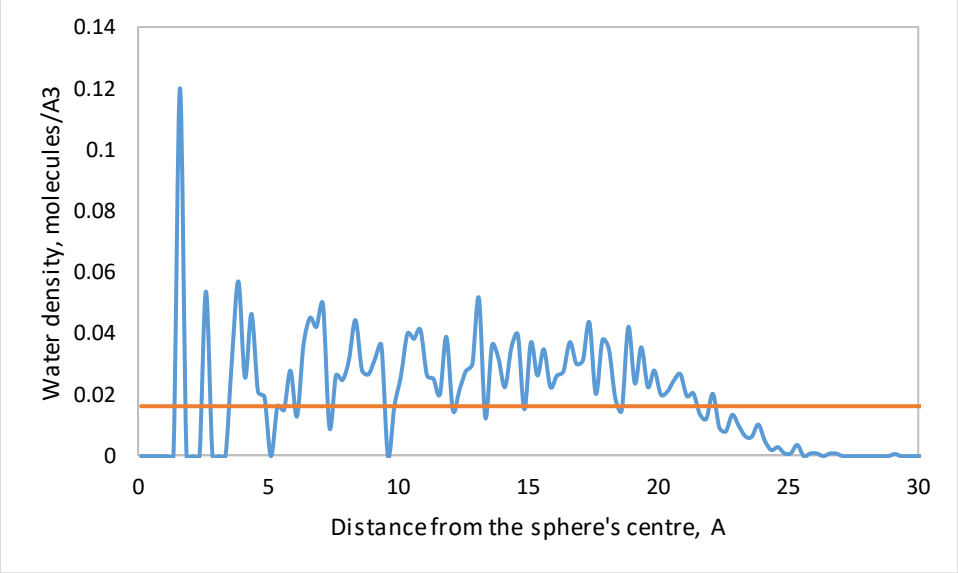

Figure 9. Water density in spherical coordinates for the system at 10 MPa CO_2 pressure. Horizontal line shows half of water's normal density.

Spheres circumscribed around water droplets and their relative positions with respect to the surfaces are presented in Figure 10 and Figure 11. As expected, circumscribed spheres average fuzzy borders of the droplets eliminating the directional bias.

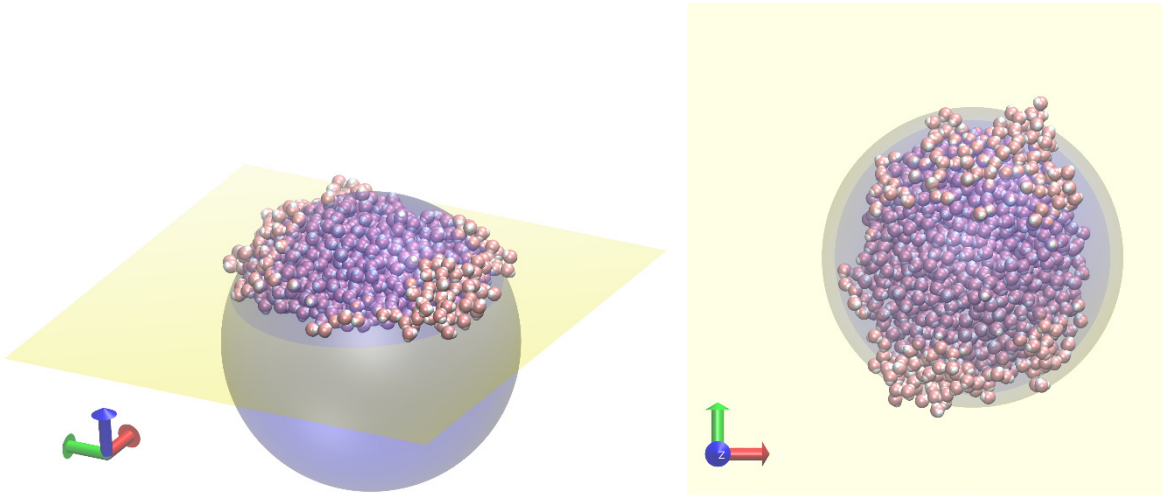

Figure 10. Water droplet and its circumscribed sphere on the quartz surface at 4 MPa CO_2 pressure, isometric view (left) and top view (right). Orange balls are oxygen atoms and white balls are hydrogen atoms of the TIP4P/2005 water.

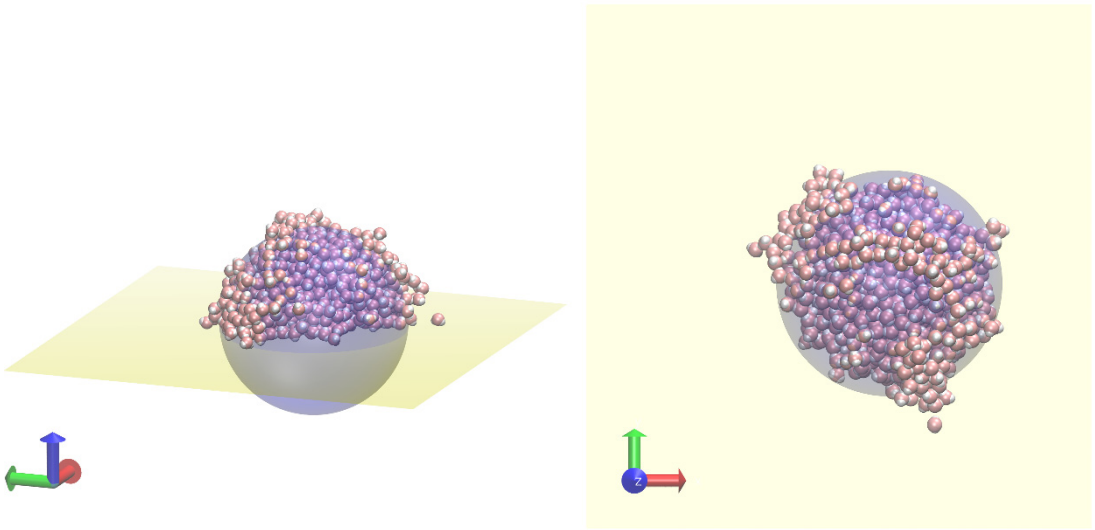

Figure 11. Water droplet and its circumscribed sphere on the quartz surface at 10 MPa CO_2 pressure, isometric view (left) and top view (right). Orange balls are oxygen atoms and white balls are hydrogen atoms of the TIP4P/2005 water.

Iso-density charts used to compare results of the contact angle calculations with the circumscribed sphere method are shown in Figure 12 and Figure 13. The circumscribed spheres almost average the iso-density constructed in cylindrical coordinates, especially at 10 MPa CO_2 pressure. The contact angles calculated using three sets of data points (5, 7 and 9) average the iso-densities close to the surface and show good agreement between each other (error bars are less than 7%): 69.0° (+/-4.7°) and 92.6° (+/-2.6°) for systems at 4 and 10 MPa of CO_2 pressure, respectively.

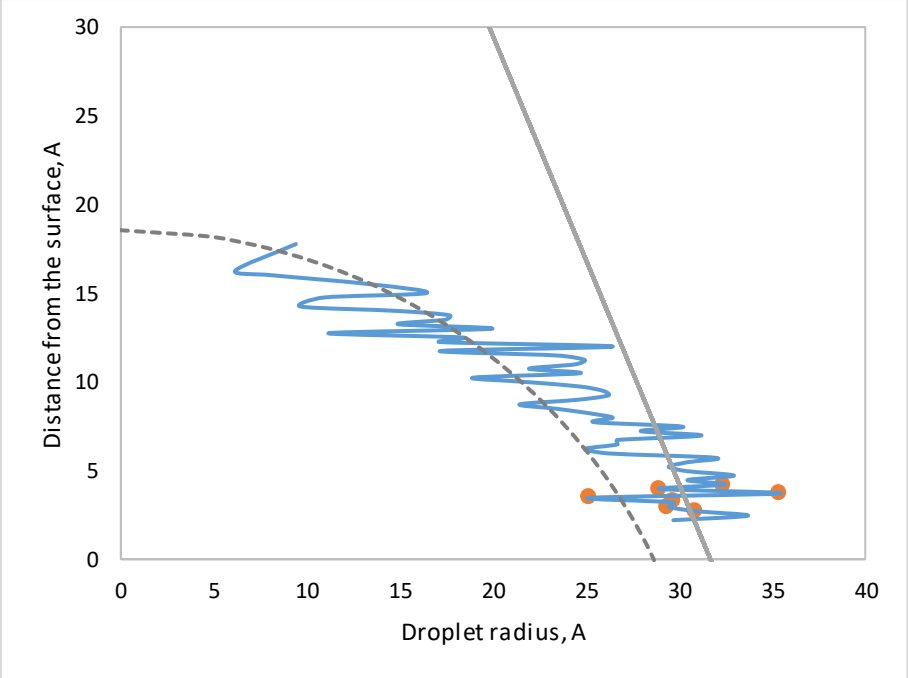

Figure 12. Iso-density chart constructed in cylindrical coordinates for a water droplet on a pristine quartz surface at 4 MPa CO_2 pressure. Blue line shows half of water normal density. Red dots depict data points used to fit the tangential line, the straight line (5, 7 and 9 points were used for the averaging, the case for 7 points is shown). The dashed line shows the circumscribed sphere contour found in the spherical coordinates.

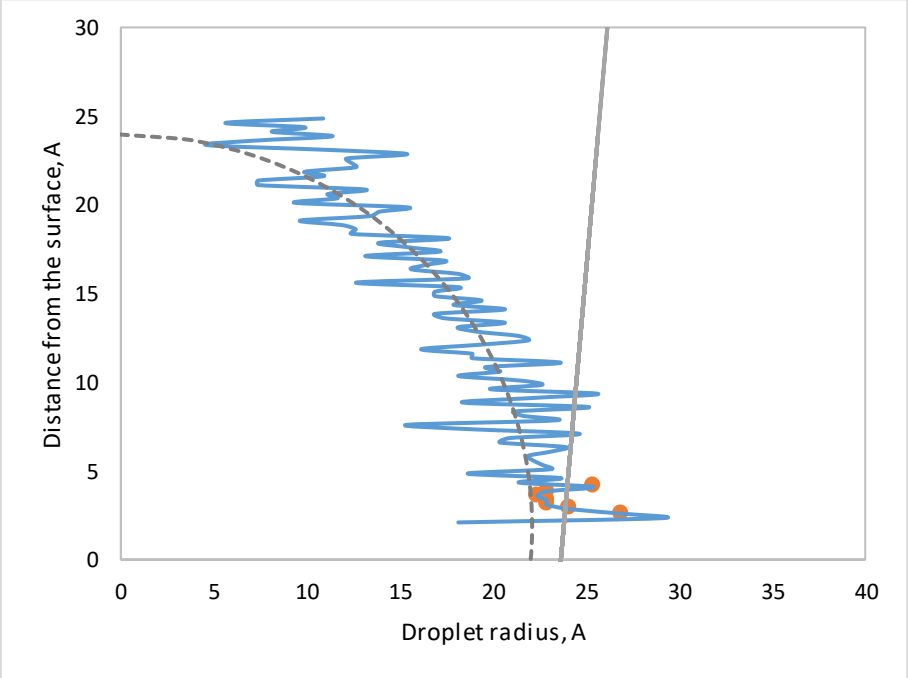

Figure 13. Iso-density chart constructed in cylindrical coordinates for a water droplet on a pristine quartz surface at 10 MPa CO_2 pressure. Blue line shows half of water normal density. Red dots depict data points used to fit the tangential line, the straight line (5, 7 and 9 points were used for the averaging, the case for 7 points is shown). The dashed line shows the circumscribed sphere contour found in the spherical coordinates.

Obtained numerical parameters and overall agreement between two methods used to determine the contact angle, as well as visual inspection of the simulation snapshots and the diagrammatic data demonstrate that the spheroidal constructions and the spherical coordinate system have promising potential in the area. The algorithms proposed here are simple and can be intuitively understood, and the required computational effort to analyse a simulation snapshot is minor.

Conclusions

The concept of how to determine computational contact angles of a liquid droplet resting on a solid surface from individual snapshots of molecular dynamics simulations have been formulated, implemented and analysed in this study. Spherical coordinates to circumscribe a sphere around given configuration of water molecules form the basis of the method, which is thus natural and consistent with the droplet's geometric computational framework. The method also shows good agreement with the iso-density chart method which was applied here.

The contact angle of a water droplet on the most stable 6-member ellipse-like rings (001) surface of α-quartz, which was reconstructed here using classical molecular dynamics, was found to be 66 and 95° at 4 and 10 MPa of CO_2 pressure, respectively. Comparison with previously done study [7] shows that the 6-member ellipse-like rings surface is more hydrophobic than the 6-member triangle-like rings surface of α-quartz (c.f. contact angles at 10 MPa of CO_2 pressure 95° and 80°, respectively).

Procedures used to compute the contact angles on basis of molecular dynamics output have deficiencies and limitations when applied on their own. The circumscribed sphere method in its current implementation is best suited for hydrophobic surfaces, but otherwise sensitive to the integrity of the water droplet and may need pre-processing for droplets with poorly defined borders to remove escaped (from the main body of water) molecules. The iso-density chart method is less sensitive to integrity, but local in nature and thus requires caution when fitting the tangential line. Without a universal unbiased method, a combination of several approaches can complement each other in providing a confident estimate of the contact angle from molecular dynamics computations.

Acknowledgments

This work was supported by resources provided by the Pawsey Supercomputing Centre with funding from the Australian Government and the Government of Western Australia.

References

1. IPCC *Carbon Dioxide Capture and Storage*; Intergovernmental Panel on Climate Change: 2005, 2005.
2. Iglauer, S.; Al-Yaseri, A. Z.; Rezaee, R.; Lebedev, M., CO2 wettability of caprocks: Implications for structural storage capacity and containment security. *Geophysical Research Letters* **2015,** *42* (21), 9279-9284.
3. Iglauer, S., CO2–Water–Rock Wettability: Variability, Influencing Factors, and Implications for CO2 Geostorage. *Accounts of Chemical Research* **2017,** *50* (5), 1134-1142.
4. Iglauer, S.; Pentland, C. H.; Busch, A., CO2 wettability of seal and reservoir rocks and the implications for carbon geo-sequestration. *Water Resources Research* **2014,** *51* (1), 729-774.
5. Giovambattista, N.; Debenedetti, P. G.; Rossky, P. J., Effect of Surface Polarity on Water Contact Angle and Interfacial Hydration Structure. *The Journal of Physical Chemistry B* **2007,** *111* (32), 9581-9587.
6. Bagherzadeh, S. A.; Englezos, P.; Alavi, S.; Ripmeester, J. A., Influence of Hydrated Silica Surfaces on Interfacial Water in the Presence of Clathrate Hydrate Forming Gases. *The Journal of Physical Chemistry C* **2012,** *116* (47), 24907-24915.
7. Iglauer, S.; Mathew, M. S.; Bresme, F., Molecular dynamics computations of brine–CO2 interfacial tensions and brine–CO2–quartz contact angles and their effects on structural and residual trapping mechanisms in carbon geo-sequestration. *Journal of Colloid and Interface Science* **2012,** *386* (1), 405-414.
8. McCaughan, J.; Iglauer, S.; Bresme, F., Molecular Dynamics Simulation of Water/CO2-quartz Interfacial Properties: Application to Subsurface Gas Injection. *Energy Procedia* **2013,** *37*, 5387-5402.
9. Chen, C.; Wan, J.; Li, W.; Song, Y., Water contact angles on quartz surfaces under supercritical CO2 sequestration conditions: Experimental and molecular dynamics simulation studies. *International Journal of Greenhouse Gas Control* **2015,** *42*, 655-665.
10. Liu, S.; Yang, X.; Qin, Y., Molecular dynamics simulation of wetting behavior at CO2/water/solid interfaces. *Chinese Science Bulletin* **2010,** *55* (21), 2252-2257.
11. Chen, C.; Zhang, N.; Li, W.; Song, Y., Water Contact Angle Dependence with Hydroxyl Functional Groups on Silica Surfaces under CO2 Sequestration Conditions. *Environmental Science & Technology* **2015,** *49* (24), 14680-14687.
12. Chen, C.; Chai, Z.; Shen, W.; Li, W.; Song, Y., Wettability of Supercritical CO2–Brine–Mineral: The Effects of Ion Type and Salinity. *Energy & Fuels* **2017,** *31* (7), 7317-7324.
13. Chen, C.; Chai, Z.; Shen, W.; Li, W., Effects of Impurities on CO2 Sequestration in Saline Aquifers: Perspective of Interfacial Tension and Wettability. *Industrial & Engineering Chemistry Research* **2018,** *57* (1), 371-379.
14. Tenney, C. M.; Cygan, R. T., Molecular Simulation of Carbon Dioxide, Brine, and Clay Mineral Interactions and Determination of Contact Angles. *Environmental Science & Technology* **2014,** *48* (3), 2035-2042.
15. Tsuji, S.; Liang, Y.; Kunieda, M.; Takahashi, S.; Matsuoka, T., Molecular Dynamics Simulations of the CO2-Water-silica Interfacial Systems. *Energy Procedia* **2013,** *37*, 5435-5442.
16. Liang, Y.; Tsuji, S.; Jia, J.; Tsuji, T.; Matsuoka, T., Modeling CO2–Water–Mineral Wettability and Mineralization for Carbon Geosequestration. *Accounts of Chemical Research* **2017,** *50* (7), 1530-1540.

17. Javanbakht, G.; Sedghi, M.; Welch, W.; Goual, L., Molecular Dynamics Simulations of CO2/Water/Quartz Interfacial Properties: Impact of CO2 Dissolution in Water. *Langmuir* **2015,** *31* (21), 5812-5819.
18. Deng, Y.; Xu, L.; Lu, H.; Wang, H.; Shi, Y., Direct measurement of the contact angle of water droplet on quartz in a reservoir rock with atomic force microscopy. *Chemical Engineering Science* **2018,** *177*, 445-454.
19. Ravipati, S.; Aymard, B.; Kalliadasis, S.; Galindo, A., On the equilibrium contact angle of sessile liquid drops from molecular dynamics simulations. *The Journal of Chemical Physics* **2018,** *148* (16), 164704.
20. Chen, Y.-W.; Cao, C.; Cheng, H.-P., Finding stable α-quartz (0001) surface structures via simulations. *Applied Physics Letters* **2008,** *93* (18), 181911.
21. de Leeuw, N. H.; Higgins, F. M.; Parker, S. C., Modeling the Surface Structure and Stability of α-Quartz. *The Journal of Physical Chemistry B* **1999,** *103* (8), 1270-1277.
22. Eder, S. D.; Fladischer, K.; Yeandel, S. R.; Lelarge, A.; Parker, S. C.; Søndergård, E.; Holst, B., A Giant Reconstruction of α-quartz (0001) Interpreted as Three Domains of Nano Dauphine Twins. *Scientific Reports* **2015,** *5*, 14545.
23. Feya, O. D.; Wang, Q.; Lepeshkin, S. V.; Baturin, V. S.; Uspenskii, Y. A.; Oganov, A. R., Tetrahedral honeycomb surface reconstructions of quartz, cristobalite and stishovite. *Scientific Reports* **2018,** *8* (1), 11947.
24. Malyi, O. I.; Kulish, V. V.; Persson, C., In search of new reconstructions of (001) α-quartz surface: a first principles study. *RSC Advances* **2014,** *4* (98), 55599-55603.
25. Franks, F., *Water: A Matrix of Life: Edition 2*. The Royal Society of Chemistry: 2000.
26. Todorov, I. T.; Smith, W.; Trachenko, K.; Dove, M. T., DL_POLY_3: new dimensions in molecular dynamics simulations via massive parallelism. *Journal of Materials Chemistry* **2006,** *16* (20), 1911-1918.
27. Bush, I. J.; Todorov, I. T.; Smith, W., A DAFT DL_POLY distributed memory adaptation of the Smoothed Particle Mesh Ewald method. *Computer Physics Communications* **2006,** *175* (5), 323-329.
28. Humphrey, W.; Dalke, A.; Schulten, K., VMD: Visual molecular dynamics. *Journal of Molecular Graphics* **1996,** *14* (1), 33-38.
29. Momma, K.; Izumi, F., VESTA: a three-dimensional visualization system for electronic and structural analysis. *Journal of Applied Crystallography* **2008,** *41* (3), 653-658.
30. Swope, W. C.; Andersen, H. C.; Berens, P. H.; Wilson, K. R., A computer simulation method for the calculation of equilibrium constants for the formation of physical clusters of molecules: Application to small water clusters. *The Journal of Chemical Physics* **1982,** *76* (1), 637-649.
31. Hoover, W. G., Canonical dynamics: Equilibrium phase-space distributions. *Physical Review A* **1985,** *31* (3), 1695-1697.
32. Nosé, S., A molecular dynamics method for simulations in the canonical ensemble. *Molecular Physics* **1984,** *52* (2), 255-268.
33. Essmann, U.; Perera, L.; Berkowitz, M. L.; Darden, T.; Lee, H.; Pedersen, L. G., A smooth particle mesh Ewald method. *The Journal of Chemical Physics* **1995,** *103* (19), 8577-8593.
34. Darden, T.; York, D.; Pedersen, L., Particle mesh Ewald: An N·log(N) method for Ewald sums in large systems. *The Journal of Chemical Physics* **1993,** *98* (12), 10089-10092.
35. van Beest, B. W. H.; Kramer, G. J.; van Santen, R. A., Force fields for silicas and aluminophosphates based on ab initio calculations. *Physical Review Letters* **1990,** *64* (16), 1955-1958.
36. Abascal, J. L. F.; Vega, C., A general purpose model for the condensed phases of water: TIP4P/2005. *The Journal of Chemical Physics* **2005,** *123* (23), 234505.
37. Harris, J. G.; Yung, K. H., Carbon Dioxide's Liquid-Vapor Coexistence Curve And Critical Properties as Predicted by a Simple Molecular Model. *The Journal of Physical Chemistry* **1995,** *99* (31), 12021-12024.

38. Buckingham, R. A., The classical equation of state of gaseous helium, neon and argon. *Proceedings of the Royal Society of London. Series A. Mathematical and Physical Sciences* **1938,** *168* (933), 264-283.
39. Lorentz, H. A., Ueber die Anwendung des Satzes vom Virial in der kinetischen Theorie der Gase. *Annalen der Physik* **1881,** *248* (1), 127-136.
40. Berthelot, D., Sur le mélange des gaz. *Comptes rendus hebdomadaires des séances de l'Académie des Sciences* **1898,** *126*, 1703-1855.
41. Levien, L.; Prewitt, C. T.; Weidner, D. J., Structure and elastic properties of quartz at pressure. *American Mineralogist* **1980,** *65* (9-10), 920-930.
42. Adeagbo, W. A.; Doltsinis, N. L.; Klevakina, K.; Renner, J., Transport Processes at α-Quartz–Water Interfaces: Insights from First-Principles Molecular Dynamics Simulations. *ChemPhysChem* **2008,** *9* (7), 994-1002.
43. webbook.nist.gov NIST Chemistry WebBook. https://webbook.nist.gov/chemistry/.
44. Bikkina, P. K., Contact angle measurements of CO2-water-quartz/calcite systems in the perspective of carbon sequestration. *International Journal of Greenhouse Gas Control* **2011,** *5* (5), 1259-1271.